



HAL
open science

Wall-pressure spectral model including the adverse pressure gradient effects

Yannick Rozenberg, Gilles Robert, Stéphane Moreau

► **To cite this version:**

Yannick Rozenberg, Gilles Robert, Stéphane Moreau. Wall-pressure spectral model including the adverse pressure gradient effects. *AIAA Journal*, 2012, 50 (10), pp.2168-2179. 10.2514/1.J051500 . hal-00780119

HAL Id: hal-00780119

<https://hal.science/hal-00780119>

Submitted on 3 Mar 2014

HAL is a multi-disciplinary open access archive for the deposit and dissemination of scientific research documents, whether they are published or not. The documents may come from teaching and research institutions in France or abroad, or from public or private research centers.

L'archive ouverte pluridisciplinaire **HAL**, est destinée au dépôt et à la diffusion de documents scientifiques de niveau recherche, publiés ou non, émanant des établissements d'enseignement et de recherche français ou étrangers, des laboratoires publics ou privés.

Wall Pressure Spectral Model Including the Adverse Pressure Gradient Effects

Yannick Rozenberg ¹ and Gilles Robert ²
LMFA - Ecole Centrale de Lyon, 69134 Écully Cedex, France

Stéphane Moreau ³
Université de Sherbrooke, Sherbrooke, QC, J1K2R1, Canada

An empirical model to predict the wall-pressure fluctuations spectra beneath adverse pressure gradient flows is presented. It is based on Goody's model which already incorporates the effect of Reynolds number but is limited to zero-pressure gradient flows. The extension relies on 6 test-cases from 5 experimental or numerical studies covering a large range of Reynolds number, $5.6 \times 10^2 < R_\theta < 1.72 \times 10^4$, in both internal (channel) and external (airfoil) flows. A review of the boundary layer parameters characterizing the pressure gradient effects is provided and the more relevant ones are introduced as new variables in the model. The method is then compared to the zero-pressure gradient model it is derived from. The influence of the pressure gradient on the wall-pressure spectrum is discussed. Finally, the method is applied to provide input data of radiated trailing-edge noise model by means of an aeroacoustic analogy, namely Amiet's theory of turbulent boundary layer past a trailing edge. The results are compared to experimental data obtained in open-jet anechoic wind tunnel.

¹ Research Engineer, yannick.rozenberg@ec-lyon.fr

² Senior Lecturer, gilles.robert@ec-lyon.fr

³ Professor, GAUS, Mechanical Engineering Department, stephane.moreau@usherbrooke.ca

NOMENCLATURE

b	= Corcos' constant
C_1, C_2, C_3	= Goody's model constants
C_f	= skin friction coefficient
C_p	= pressure coefficient
C^+	= constant in the log law
c_0	= speed of sound [m.s ⁻¹]
g	= wall-law function
h	= Coles' wake-law function
$H = \delta^*/\theta$	= shape factor
k	= wavenumber [m ⁻¹]
l_y	= coherence spanwise length scale [m]
p	= pressure [Pa]
$\overline{p^2}$	= mean square unsteady pressure [Pa ²]
R_T	= ratio of timescales of pressure
R_θ	= Reynolds number based on U_e and θ
U_c	= convection velocity [m.s ⁻¹]
U_e	= external velocity [m.s ⁻¹]
U_i	= inlet velocity [m.s ⁻¹]
u_τ	= friction velocity [m.s ⁻¹]
β_C	= Clauser's parameter
Δ	= Zagarola & Smits' parameter
δ	= boundary layer thickness [m]
δ^*	= boundary layer displacement thickness [m]
θ	= boundary layer momentum thickness [m]
κ	= von Kármán constant
ν	= kinematic viscosity [s ² .m ⁻²]

Π	= wake strength parameter
ρ_0	= air density [kg.m ⁻³]
τ_w	= wall shear stress [Pa]
τ_{max}	= maximum shear stress [Pa]
ω	= angular frequency
$\tilde{\omega}$	= Strouhal number based on external variables
Φ_{pp}	= power spectral density of surface pressure fluctuations [Pa ² /Hz]
$\bar{\cdot}$	= mean value

I. Introduction

Wall pressure fluctuations induced by flow over solid surface result from turbulent velocity fluctuations in the turbulent boundary layer. Studying and modeling them is of fundamental and practical interests. The diffraction of wall pressure fluctuations near edges yields the so-called trailing-edge noise [1–4] which constitutes the most basic aeroacoustic mechanism of a surface of limited extent embedded in a clean flow. Likewise, the vibration of a panel induced by the pressure fluctuations leads to the generation of acoustic radiation into an aircraft cabin, for example, and the knowledge of the wall-pressure statistics is required to evaluate the passenger disturbance during the flight. Taking the divergence of the incompressible Navier-Stokes equations and performing a Reynolds decomposition leads to the following Poisson’s equation that relates the pressure fluctuations (p) to the fluctuating velocity (u_i) and the mean velocity (U_i) :

$$\frac{1}{\rho} \frac{\partial^2 p}{\partial x_i^2} = -2 \frac{\partial \bar{U}_i}{\partial x_j} \frac{\partial u_j}{\partial x_i} - \frac{\partial^2 (u_i u_j - \bar{u}_i \bar{u}_j)}{\partial x_i \partial x_j}. \quad (1)$$

As noted by Bull [5], the integral solution of this equation implies that the pressure is determined by contributions from all parts of the velocity field. Since there is no universal law to describe the velocity field in the different layers of the boundary layer, since the turbulent eddies are convected at different velocities depending on their distance to the wall and since the wall pressure is influenced by the velocity fluctuations in the whole boundary layer, the pressure field structure is inevitably complex. Accurate predictions of such pressure fields have been performed, using direct numeri-

cal simulations (DNS) or large eddy simulations (LES) [6–8]. Such computations are highly time consuming and not yet affordable in complex configurations. In such cases, the flowfield is often determined by Reynolds-Averaged Navier-Stokes (RANS) simulations. Adequate post-processing coupled with statistical models has been used to determine the pressure auto-spectrum.

Lee *et al.* [9] developed a spectral modeling scheme coupled with a RANS simulation. The vertical turbulent fluctuating velocity and the gradients of the streamwise mean shear velocity were predicted from the turbulent kinetic energy. The model was then applied to an equilibrium flow with a fairly good agreement. It has been extended to non-equilibrium flows by adding a non-linear source term in the Poisson equation [10]. Based on the same idea of modeling the space-time velocity correlation using RANS data, Peltier & Hambric [11] proposed a stochastic model to predict wall-pressure spectra. The effects of pressure gradients (favorable, zero and adverse) are correctly predicted but the validation is limited to mild pressure gradients. Recently, Remmler *et al.* [12] readdress the modeling of wall-pressure spectra on the basis of Panton & Linebarger’s hypotheses [13] and input data from steady RANS simulations. The far-field acoustic pressure radiated by a highly loaded airfoil is then favorably compared with experimental data.

Another technique to predict wall-pressure spectra is a scaling that consists in the use of appropriate normalized parameters to collapse wall-pressure spectra on a single curve. Unfortunately, there is no universal scaling that collapses the pressure spectra for a large frequency range and different Reynolds numbers. For zero-pressure gradient flows, various models and normalized parameters have been proposed. The present paper aims to extend this technique to Adverse Pressure Gradient (APG) flows, such as canonical channel flows or more realistic flows around airfoils with positive angle of attack. In section II, three empirical models relying on theoretical and experimental studies are reviewed. They are limited to ZPG flows and underestimate the wall-pressure spectrum in APG configurations. Then, the effects of the APG on the turbulent boundary layer parameters are studied in section III and the more relevant parameters, characterizing the boundary layer and its history are selected. The proposed model based on Goody’s model [14] and taking into account the APG effects is presented in section IV and assessed in section V.

II. Review of empirical wall-pressure spectral models

The turbulent boundary layer is characterized by a large range of relevant length, velocity and pressure scales. A two-layer model is widely used to scale the turbulent boundary layer. The nearest flow to the wall, called the viscous sub-layer, provides a first set of length, velocity and pressure scales; the outer layer, a second one. Based on this description, Keith *et al.* [15] compared the wall-pressure spectra from various experiments corrected for spatial resolution errors [16] in a normalized form. The high-frequency range of the pressure spectra collapses when it is normalized by inner-layer scales, such as the wall shear stress τ_w for the pressure scale and ν/u_τ^2 for the timescale, with ν the kinematic viscosity and u_τ the friction velocity. For low frequencies, a collapse is observed with outer-layer scaling, such as the velocity at the boundary layer edge U_e , the boundary-layer thickness δ or the boundary-layer displacement thickness δ^* . Based on this description, three empirical wall pressure spectral (WPS) models are briefly reviewed: Amiet's model, Chase-Howe's model and Goody's model. The latter takes into account the effect of the Reynolds number. For a more detailed review of semi-empirical models for turbulent boundary layer wall-pressure spectra, the reader is invited to refer to the paper by Hwang *et al.* [17]. The wall-pressure spectra presented in the present article follow the single-sided convention: $\overline{p^2} = \int_0^\infty \Phi_{pp}(\omega) d\omega$.

A. WPS Amiet's model

Willmarth & Roos [18] have collected experimental wall-pressure fluctuations beneath a turbulent boundary layer. Based on these data, Amiet [1] proposed an analytical formulation using the outer variables:

$$\frac{\Phi_{pp}(\omega)}{\rho_0^2 \delta^* U_e^3} = 2.10^{-5} \frac{F(\tilde{\omega})}{2}, \quad (2)$$

where

$$F(\tilde{\omega}) = (1 + \tilde{\omega} + 0.217\tilde{\omega}^2 + 0.00562\tilde{\omega}^4)^{-1},$$

with $\tilde{\omega} = \omega \delta^* / U_e$ and $0.1 < \tilde{\omega} < 20$.

Figure 1 compares the model with data collected by Keith *et al.* [15] and scaled by outer variables. It represents a good mean-value but the data are spread out, in particular at high frequencies.

At low frequencies, data collapse except Choi & Moin’s ones. It is to be noted that the latter are the only one coming from a numerical simulation at a low Reynolds number $R_\theta = 1332$ based on the external velocity and the momentum thickness.

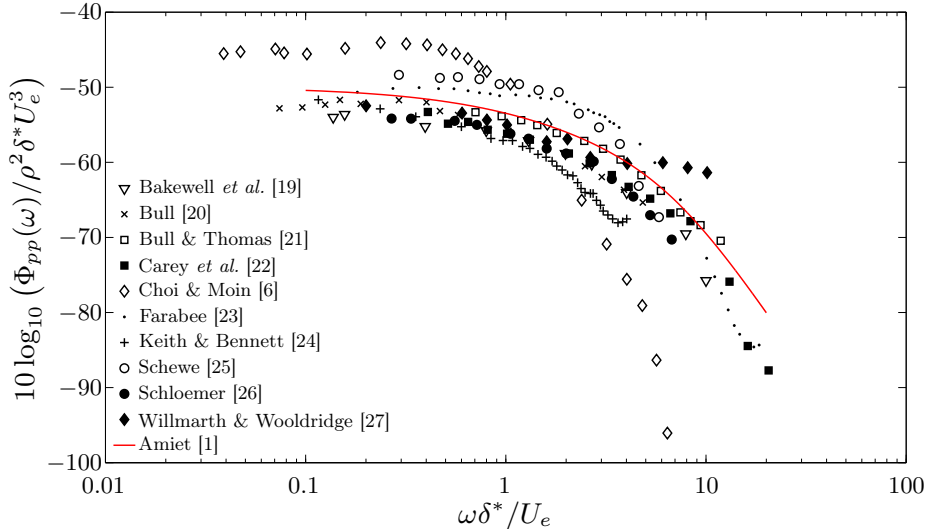


Fig. 1: Wall pressure spectra scaled by outer variables. Amiet’s WPS model [1] vs data collected by Keith *et al.* [15] and corrected for spatial resolution errors.

B. WPS Chase-Howe’s model

Based on the theoretical model developed by Chase [28], Howe describes the spectral behavior of the wall-pressure field at low Mach number in the convective domain, namely for $k \gg \omega/c_0$ [29]. Based on mixed variables, Howe suggests the following formulation:

$$\frac{\Phi_{pp}(\omega)U_e}{\tau_w^2 \delta^*} = \frac{2\tilde{\omega}^2}{[\tilde{\omega}^2 + 0.0144]^{3/2}} \quad (3)$$

As observed by Keith [15], the use of mixed variables to define a scaling law is worthwhile, since the data have a better collapse than with outer variables. Experimental wall-pressure spectra exhibit 3 slopes: a positive slope at low frequencies, a slight negative slope in the overlap region and a high negative slope at high frequencies. The Chase-Howe spectrum is proportional to ω^2 at low frequencies. It varies as ω^{-1} at higher frequencies, corresponding to the wall-pressure spectra behavior in the overlap region where both inner and outer-layer scaling can be used to make the data

collapse [30]. However, it does not include the third slope at higher frequencies as experimentally and theoretically observed (cf. Fig. 2).

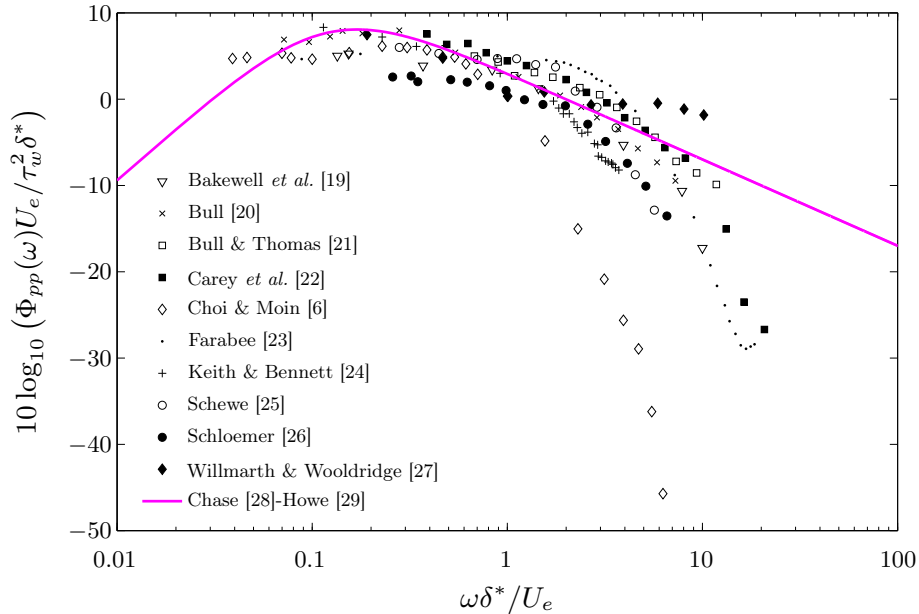


Fig. 2: Wall pressure spectra scaled by mixed variables. Chase [28]-Howe [29] model vs data collected by Keith *et al.* [15] and corrected for spatial resolution errors.

C. WPS Goody's model

The discrepancies observed at high frequencies in Fig. 2 are attributed to Reynolds number effects. Goody's objective is to take into account this effect of the Reynolds number using an empirical approach [14]. Based on Chase-Howe's model and the experimental results of seven research teams, he modified Eq. 3 to agree better with the experimental data. A term was added to the denominator so that spectral levels decay as ω^{-5} when $\omega \rightarrow \infty$. The exponents in the denominator were changed to better agree with the measured pressure spectral behavior in the overlap range (middle frequencies with a $\omega^{-0.7}$ decay). Moreover, the only effect of Reynolds number on the shape of the wall-pressure spectrum is to increase the size of the overlap range. Finally, δ is preferred to δ^* because the largest coherent structures are in the order of δ . The final form of the semi-empirical

model is:

$$\frac{\Phi_{pp}(\omega)U_e}{\tau_w^2\delta} = \frac{C_2(\omega\delta/U_e)^2}{\left[(\omega\delta/U_e)^{0.75} + C_1\right]^{3.7} + [C_3(\omega\delta/U_e)]^7}, \quad (4)$$

where C_1 , C_2 and C_3 are empirical constants with the following recommended value: 0.5, 3.0 and $1.1R_T^{-0.57}$ respectively, with $R_T = (\delta/U_e)/(\nu/u_\tau^2) = (u_\tau\delta/\nu)\sqrt{C_f/2}$ the ratio of the outer to inner boundary layer time scale.

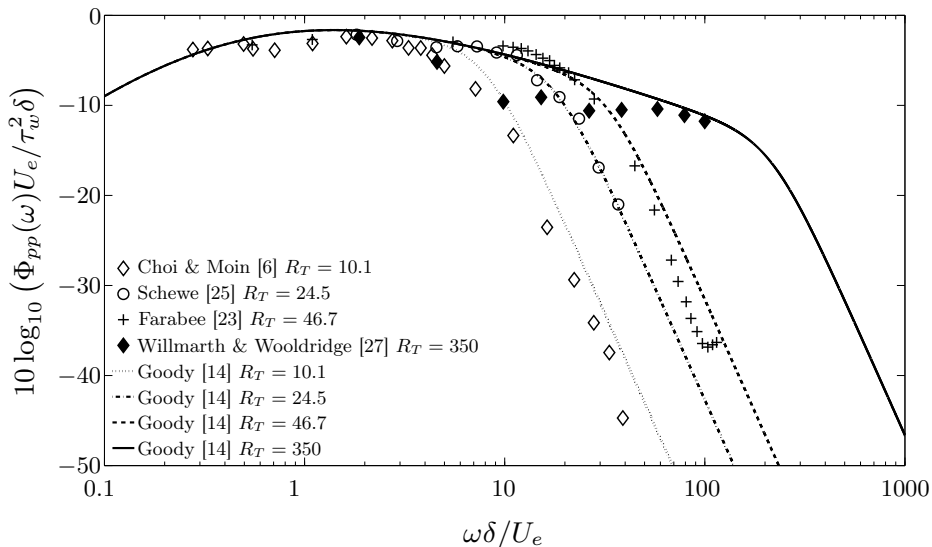


Fig. 3: Wall pressure spectra scaled by mixed variables. Goody’s model [14] vs data collected by Keith *et al.* [15] and corrected for spatial resolution errors.

Hwang *et al.* concluded in their review of empirical wall-pressure spectral models [17] that Goody’s model shows the best agreement with experiments. Goody has captured the spectral features correctly for zero-pressure gradient turbulent boundary layer flows over a wide range of Reynolds number. As observed in Fig. 3, the discrepancies at high frequencies are related to the ratio of outer-layer-to-inner-layer timescale R_T and the cut-off frequency is well predicted. Nevertheless, the model is limited to canonical flows, such as pipe flow and turbulent boundary layer over flat plate.

III. Adverse pressure gradient effects on the turbulent boundary-layer

In many applications, the turbulent boundary layer encounters an adverse mean-pressure gradient. This is the case for example on the suction side of a profile or a blade, just upstream of

the trailing edge. The spectrum of the wall-pressure fluctuations at this position is of practical interest for trailing-edge noise prediction using analytical models, as long as the boundary layer remains attached. Empirical models reviewed in section II are no longer suited to such flows. In the following section, the effects of the adverse pressure gradient on pressure fluctuations statistics are presented and 6 reference spectra from 5 numerical and/or experimental studies are selected to find some parameters characterizing the pressure-gradient effects and the boundary layer history, in order to add an APG effect into Goody's model.

A. Effects on the pressure statistics

In 1967, Schloemer [26] experimentally observed the strong effect of the mean-pressure gradient on the wall-pressure fluctuations. Spectral levels were increased for positive pressure gradient boundary layers. This is not only caused by the thickening of the boundary layer, because this trend is also observed when the wall-pressure spectra are scaled with the boundary layer displacement thickness (cf. Fig. 4). Results obtained by Na & Moin [7] from direct numerical simulation of a pipe flow with pressure gradients, created by prescribed vertical velocity distributions along the upper boundary, are also plotted. The adverse pressure effects can lead to an increase of 10 dB at low frequency. If this effect is not taken into account in the trailing-edge noise prediction, it would lead to a dramatic underestimate of the noise, since it is directly proportional to the wall-pressure spectrum in the analytical models proposed by Howe and Amiet. To build a new empirical model, parameters that characterize pressure gradients and their influence on the wall-pressure statistics will be defined.

B. Test-cases definition

The purpose of the present study is to propose an empirical wall pressure spectral model using boundary layer parameters and taking into account the adverse-pressure gradient effect. Test-cases have to be fully-documented to provide inner and outer boundary-layer variables and wall-pressure spectra. Such test-cases are not common in the scientific literature. Five studies have been selected, three are pipe flow turbulent boundary layers and two are turbulent boundary layers on loaded profiles:

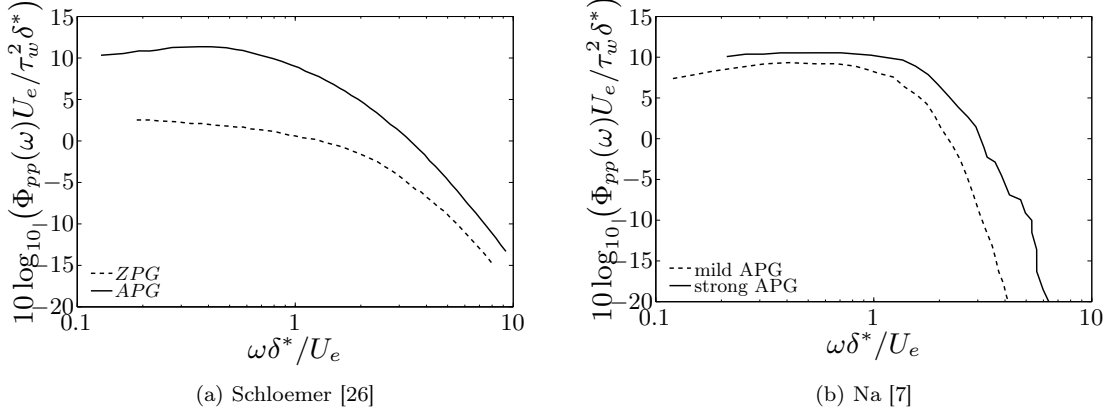


Fig. 4: Wall-pressure spectra scaled with mixed variables: adverse pressure gradient (APG) effect.

- Pipe flows:
 - experimental study by Schloemer [26]
 - numerical study using DNS by Na & Moin [7, 31]
 - experimental results [32] and RANS simulations of a pipe flow with favorable and adverse pressure gradients
- Airfoils:
 - experimental results [33, 34] and RANS simulations on 2 loaded profiles presented below

1. Schloemer's data

Using flush-mounted transducers, Schloemer [26] measured the pressure fluctuations at the bottom wall of a low-turbulence subsonic wind-tunnel. At the top wall, a half-airfoil section was attached to obtain favorable or adverse pressure gradients at the transducer position. Mean velocity profiles were obtained by single hot-wire measurements. For a given pressure gradient, when the wall-pressure spectra was normalized by a third power of the external velocity U_e and plotted as a function of Strouhal number based on the boundary-layer displacement thickness, a good collapse was observed. The boundary layer parameters measured by Schloemer are recalled in Table 1. They correspond to the normalized wall-pressure spectra presented in Fig. 4-a.

Table 1: Inner and outer boundary-layer variables from test-cases.

	Pipe flows			Airfoils		
	Schloemer	Na	ENABLE	V2 airfoil		CD airfoil
	APG	strong APG	$x = 250$ cm	RMP 17	RMP 23	RMP 25
CFD or Exp.	Exp.	CFD	CFD	CFD	CFD	CFD
U_e (m/s)	43.6	7.4	75.9	20.9	19.8	16.9
δ (m)	2.56×10^{-2}	2.62×10^{-2}	2.65×10^{-2}	2.73×10^{-3}	3.87×10^{-3}	4.98×10^{-3}
δ^* (m)	5.26×10^{-3}	4.1×10^{-3}	4.53×10^{-3}	6.97×10^{-4}	9.92×10^{-4}	2.24×10^{-3}
θ (m)	3.33×10^{-3}	2.69×10^{-3}	3.40×10^{-3}	4.05×10^{-4}	5.59×10^{-4}	8.76×10^{-4}
$H = \delta^*/\theta$	1.58	1.52	1.33	1.72	1.77	2.55
τ_w (Pa)	1.99	0.099	7.40	1.01	0.72	0.11
τ_{max} (Pa)	–	–	7.00	1.06	0.75	0.167
$\beta_C = (\theta/\tau_w)(dp/dx)$	2.07	1.14	1.11	0.19	1.68	20.9
Π	2.15	1.37	1.09	1.03	1.59	8.18
$R_\theta = U_e\theta/\nu$	9180	1332	17170	564	736	982
$\Delta = \delta/\delta^*$	4.86	6.39	5.84	3.92	3.90	2.23

2. Na & Moin's data

Na & Moin [7] performed a direct numerical simulation of a pipe flow encountering a mean-pressure gradient and corresponding to Watmuff's experiment [35]. Wall-pressure fluctuations were studied in detail: evolution of spectra, two-point velocity correlations and convection velocities were extracted along the streamwise direction. Inner and outer boundary layer parameters were given for a positive pressure gradient in Table 1.

3. ENABLE

An experimental campaign was conducted at the ECL wind tunnel to constitute an experimental database with the aerodynamic characteristics of the turbulent boundary layer and the wall pressure fluctuations for different mean pressure gradients. The test section was a square section of 0.5 m sides and a length of 6 m along the x -axis. The flow first encountered a favorable pressure gradient

(FPG) and then an adverse pressure gradient (APG), as it can be seen in Fig. 5 where the wall pressure coefficient $C_p = \frac{p - p_i}{1/2\rho_i U_i^2}$ along the streamwise direction is plotted. Measurements were made for three inflow velocities from $U_i = 25$ m/s to $U_i = 50$ m/s, but the present study will focus on the higher velocity case. The mean and fluctuating downstream components of the velocity were obtained by hot wire anemometry. The wall shear stress τ_w was also measured with a Preston tube and a Weiser probe. The Weiser probe estimate was found to be 10% lower than the Preston tube estimate. The outer diameter of the Preston tube was 1 mm. The standard curve of Patel [36] was used for calibration. As the Weiser probe was calibrated in a 2D pipe flow with a constant mean pressure gradient, values from the Weiser probe are kept here.

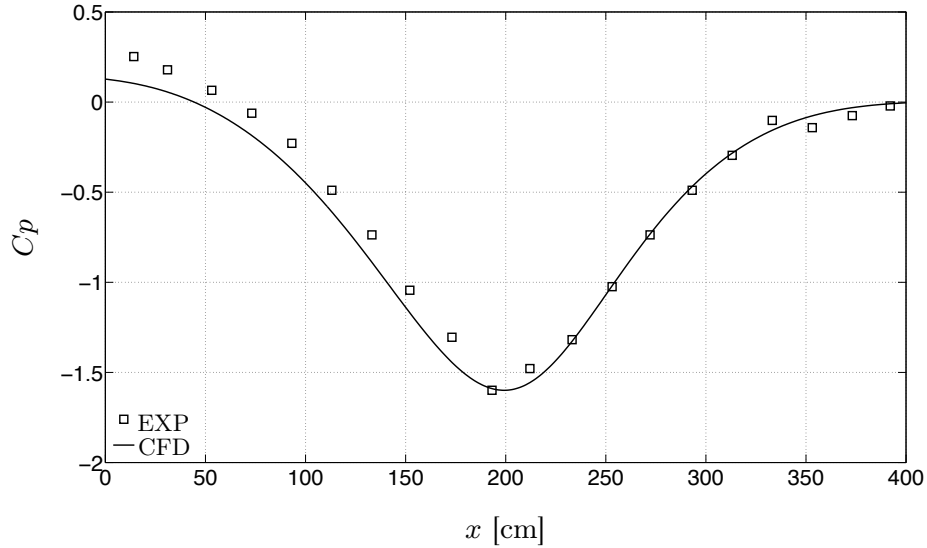


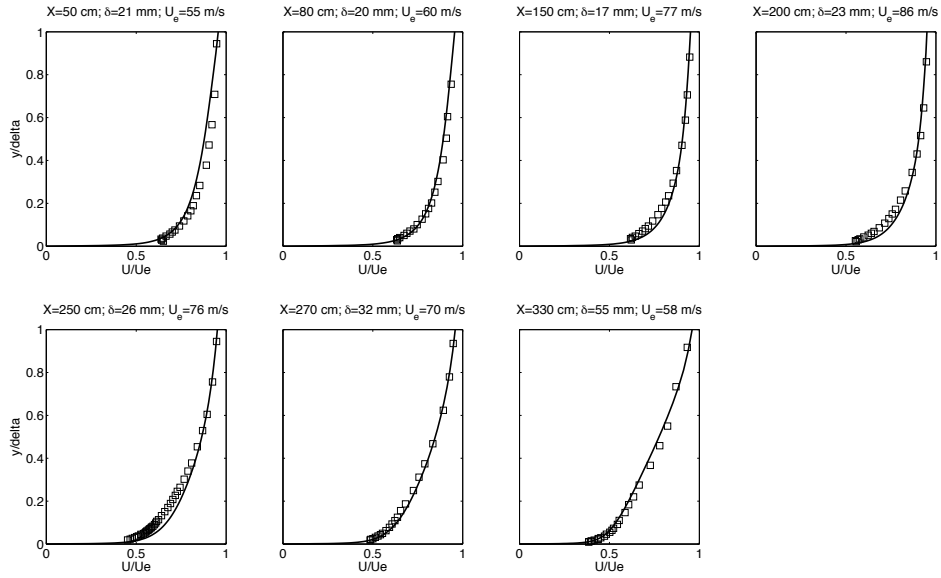
Fig. 5: Wall pressure coefficient along the streamwise direction at the bottom side of the test section.

ENABLE configuration has also been simulated with Fluent 6.2 using the $k - \omega$ SST model and assuming a 2D-flow. The pressure distribution is well-reproduced by the simulation, especially in the APG region. The velocity profiles are also compared in Fig. 6. The acceleration in the FPG region is followed by a deceleration in the APG region. In the former, the boundary layer thickness decreases whereas it increases in the latter. The CFD fluctuating velocity profiles have been deduced from the turbulent kinetic energy combined with an anisotropy factor based on the turbulent boundary layer data collected by Klebanoff [37]. Even though Klebanoff's data were

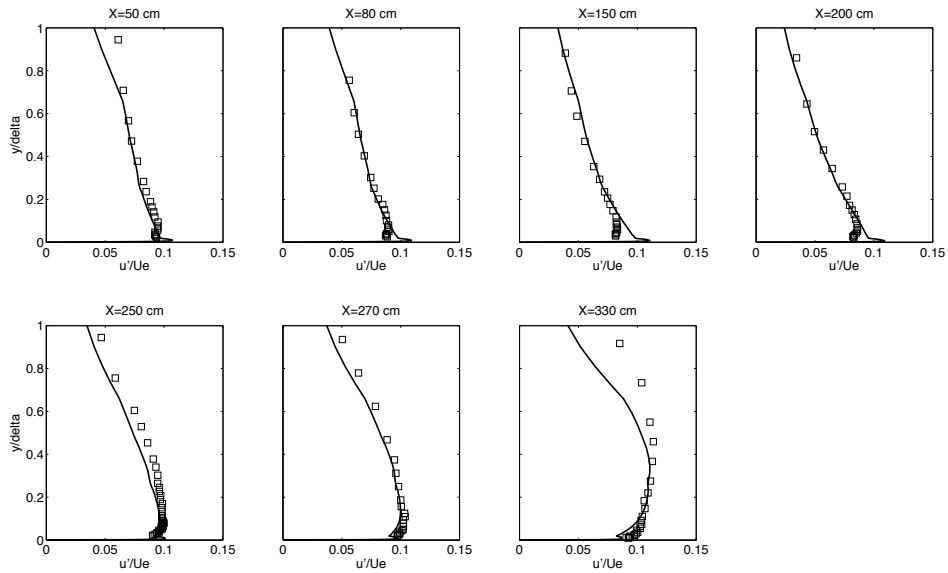
measured for a zero pressure gradient boundary layer, the anisotropy factor used for the streamwise fluctuating velocity gives quite reliable data for a 2D RANS simulation. The friction velocity is presented in Fig. 7. Values given by Fluent and based on the upwind finite-difference estimates are compared to the one deduced by the methodology proposed by Allen & Tudor [38]. A general good agreement is observed. The data are more widely spread at $x = 150$ cm and $x = 200$ cm, where disagreements of up to 10% are observed. It corresponds to the flow positions around which the pressure gradient sign changes from negative to positive. Beyond these positions, the discrepancies are less than 5% between CFD values, Allen & Tudor’s technique and experimental data obtained by the Weiser probe. The boundary layer parameters at the location $x = 250$ cm in the APG region, given by CFD and in agreement with the experiment, are summarized in Table 1.

4. *V2 airfoil*

The V2 airfoil is a low subsonic profile designed for automotive engine cooling fans. Aerodynamic and acoustic data are collected to study trailing-edge noise. The experimental setup has already been described by Moreau & Roger [34, 39]. The mock-up has a chord length of 13.6 cm and a span of 30 cm. The geometry and probes locations are presented in Fig. 8-(a). The remote microphone probes (RMPs) allow the measurements of the mean and fluctuating pressure within the frequency range 20 Hz-25 kHz. Such a probe is made with a span wise flush-mounted capillary tube and a pin hole at the measuring point. The capillary is progressively enlarged outside the mock-up till a small Electret microphone can be flush mounted [40]. Some hot-wire velocity profiles are also collected, especially in the wake, just downstream of the trailing edge. The instrumented airfoil is placed in the ECL small wind tunnel nozzle exit (13×30 cm) at a high angle of attack ($\alpha = 20^\circ$) to obtain a strong adverse pressure gradient without separation of the turbulent boundary layer. The presence of a separated flow near the trailing edge is not clear because the numerical simulation does not exhibit any plateau in the mean pressure distribution whereas the experimental results have one (cf. Fig. 9). However, the convection velocity is positive along the whole chord, suggesting an attached flow. The deflection of the jet, leading to a lower effective angle of attack than the geometric one prevents any stall at this high angle of attack. The influence of the jet on the airfoil loading has



(a) Mean-velocity profile



(b) Fluctuating-velocity profile

Fig. 6: Mean and fluctuating velocity profiles (downstream component) along the x -axis.

□ Experimental results — RANS computation

been discussed by Moreau *et al.* [41].

The experimental aerodynamic data are not sufficient to provide the boundary layer parameters

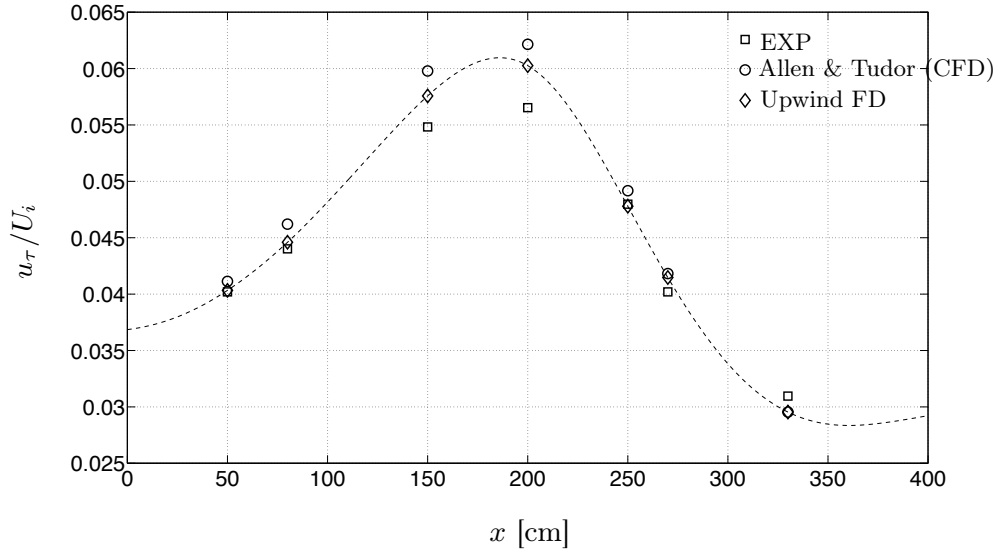


Fig. 7: Friction velocity normalized by the inlet velocity. Experimental results (Weiser probe) compared with upwind finite difference (FD) and Allen & Tudor’s method.

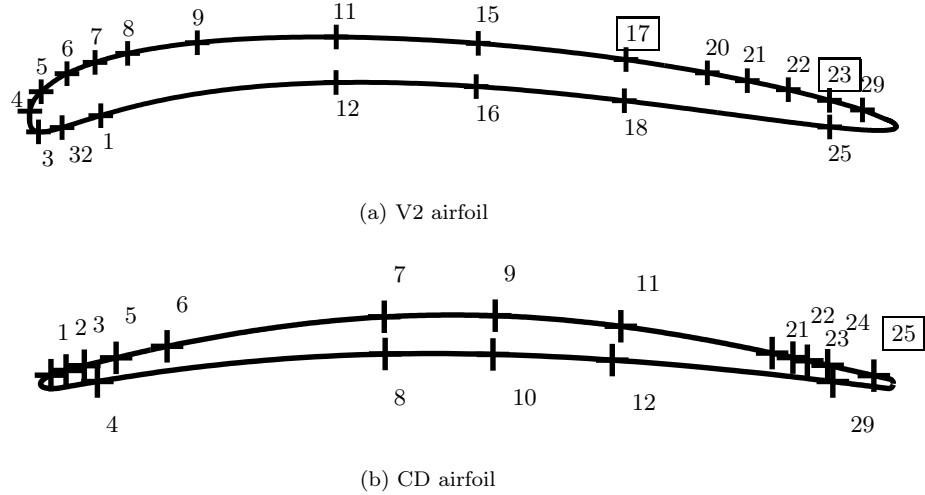


Fig. 8: Remote Microphone Probes (RMP) positions on airfoils.

needed for the normalization of wall-pressure spectra obtained in the experiment. A two-dimensional RANS simulation has been carried out using Fluent 6.2 on an unstructured grid. The nozzle of the wind-tunnel and the acoustic chamber have also been simulated to account for the installation effects [41]. The grid is composed of 63000 nodes. The mesh has been refined to obtain a dimensionless

distance to the wall, y^+ , smaller than 1 around the airfoil and to avoid the use of wall-functions. Since the $k - \omega$ SST model [42] was found to be well suited to low Reynolds number flows with adverse pressure gradients [41], it has been selected for the study. It is also well suited to capture the separation bubble near the leading edge in the boundary layer. To mimic the experimental condition, the inflow velocity is iteratively modified to obtain $U_i = 16$ m/s at the nozzle exit. To validate the simulation, three flow features have been investigated:

- the mean-pressure distribution along the suction side;
- the presence of the laminar separation bubble typical of low Reynolds number thin airfoils;
- the mean velocity profile in the wake, just downstream of the trailing edge.

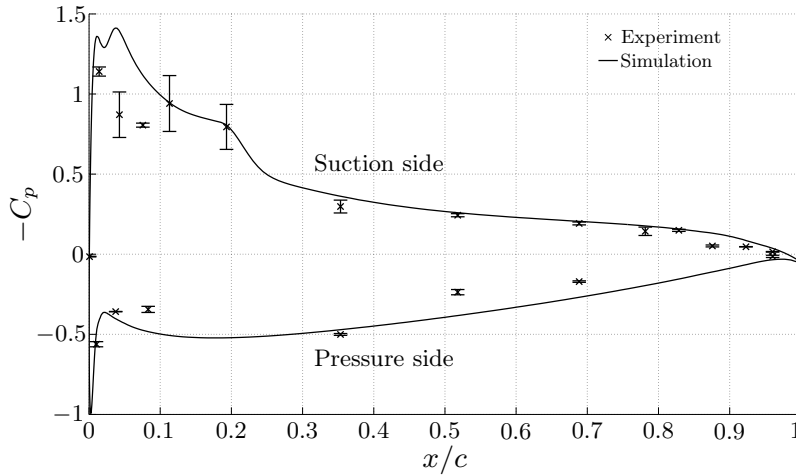


Fig. 9: Mean pressure coefficient ($-C_p$) on V2 airfoil.

The comparisons between the experimental results and the simulation are presented in Figs. 9 and 10. The experimental mean wall pressure coefficient, C_p , is well reproduced by the simulation, except near the leading-edge in the laminar separation bubble, which is found to be highly unsteady in the measurements. For the mean wall pressure, two campaigns have been carried out and the error bars point out the repeatability of the measurements. The simulation captures both position and length of the laminar separation bubble correctly. Since the transition to turbulence occurs

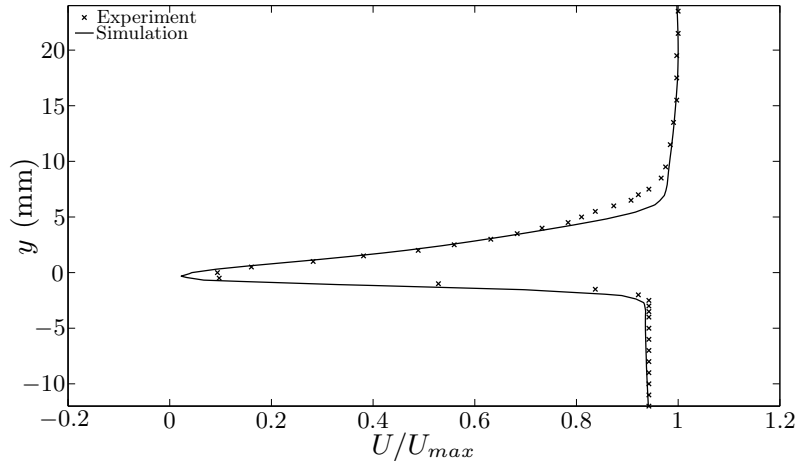


Fig. 10: Velocity profile in the wake 2 mm downstream of the trailing edge. Experimental results are obtained by single hot-wire measurements.

around the reattachment point of the laminar bubble, its presence in the simulation is crucial to obtain the realistic growth and development of the turbulent boundary layer towards the trailing edge. In Fig. 10, the velocity profile in the wake obtained by the steady simulation is very close to the experimental data. As the wake is the combination of boundary layers coming from the suction and pressure sides the boundary layers close to the trailing edge are also likely to be correctly reproduced.

The boundary layer velocity profiles are extracted along a direction normal to the wall, at the RMP locations on the suction side close to the trailing edge. To obtain the friction velocity u_τ , the methodology proposed by Allen & Tudor [38] is preferred to the direct upwind finite-difference estimates. The values are summarized in Table 1, for the 2 RMP locations studied in the next sections.

5. CD airfoil

A similar configuration was studied numerically and experimentally on a low-speed Controlled-Diffusion (CD) airfoil [41, 43]. The experimental results were obtained by Moreau & Roger [34] in the anechoic wind tunnel at ECL. The reference velocity was 16 m/s, leading to a Reynolds number based on the airfoil chord length of $Re = 1.6 \times 10^5$. The numerical results were obtained by

Christophe *et al.* [44] with the solver Ansys Fluent 12, using the $k - \omega$ SST model. The numerical results were compared with the available experimental data. As shown in Fig. 11, the pressure coefficient from the RANS simulation is in reasonable agreement with the experimental C_p . The agreement with experiment is much better in the mid-to-late suction side. The boundary layer was analyzed at $x/c = 0.98$ on the suction side, corresponding to the remote microphone probe #25 (cf. Fig. 12). The flow data were extracted on a profile normal to the local airfoil surface and are presented in Table 1. This case is critical because the boundary layer is on the verge of separating due to the strong adverse pressure gradient. The shape factor $H = \delta^*/\theta = 2.55$ is typical of such flows. The wall shear stress is obtained by Allen & Tudor’s technique and then corrected to obtain $u^+ = y^+$ in the turbulent boundary layer laminar region.

For the airfoil test-cases, the steady flow data is given by the simulations whereas the wall-pressure fluctuations come from the experimental remote microphone probe measurements.

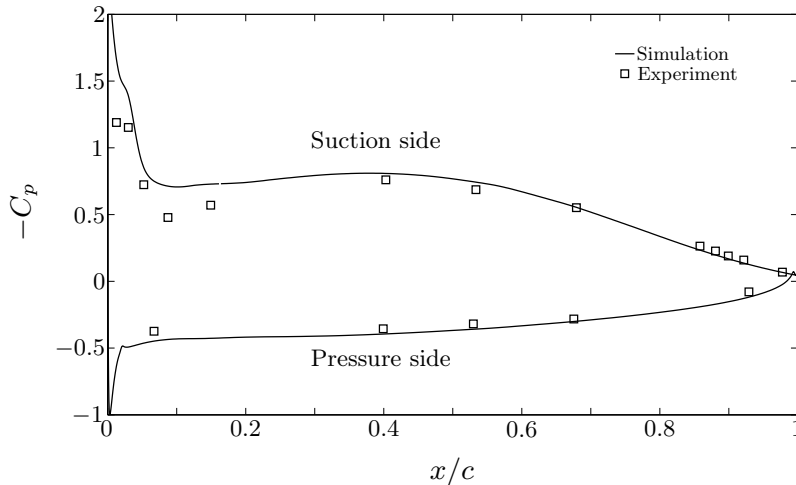


Fig. 11: Mean pressure coefficient ($-C_p$) on CD airfoil.

C. Adverse-pressure gradient markers and parameters

To build a spectral model able to take into account the adverse pressure gradient effects, we propose in the following section to review the parameters characterizing the pressure-gradient effects and the boundary layer history. This review will be illustrated by the aforementioned test-cases.

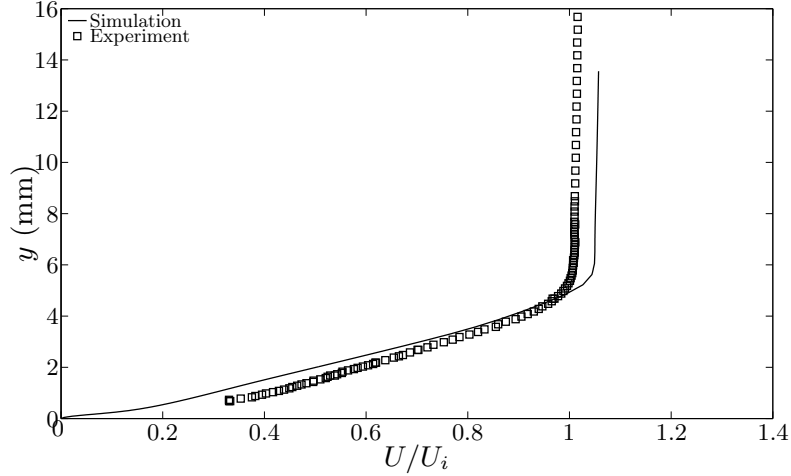


Fig. 12: Mean velocity profile in the boundary layer near the trailing edge (RMP 25)

In 1956, Coles postulated that the large-eddy structures in the outer layer of the turbulent boundary layer can be represented by a wake profile, the presence of the wall modifying mainly the viscous sub-layer and the logarithm region [45]. The turbulent boundary layer is then described by two functions g and h :

$$u^+ = g(y^+) + \frac{\Pi}{\kappa} h\left(\frac{y}{\delta}\right) \quad (5)$$

where $u^+ = U/u_\tau$ and $y^+ = yu_\tau/\nu$. Π is the wake strength parameter and the function g is the classical law of the wall:

$$g(y^+) = \frac{1}{\kappa} \ln(y^+) + C^+ \quad (6)$$

with $\kappa = 0.41$, the von Kármán constant and $C^+ = 5.1$. The function h is the law of the wake defined as:

$$h\left(\frac{y}{\delta}\right) = 2 \sin^2\left(\frac{\pi y}{2\delta}\right) \quad (7)$$

The wake strength parameter Π is found by solving the following equation derived from the normalization conditions [45]:

$$2\Pi - \ln(1 + \Pi) = \kappa \frac{U_e}{u_\tau} - \ln\left(\frac{\delta^* U_e}{\nu}\right) - \kappa C^+ - \ln \kappa \quad (8)$$

Using the results provided either by the experimental or numerical data, the wake strength parameter can be obtained easily. In Fig. 13, velocity profiles in wall units do not follow the law of the wall

at high y^+ , emphasizing the increase of the wake component. For the considered flows, the wake strength parameter varies between 1.03 and 2.15, except for the CD airfoil where its value is much higher with $\Pi = 8.18$, which denotes a boundary layer encountering a very strong adverse pressure gradient. On the suction side of the V2 airfoil, it increases in the adverse pressure gradient region from 1.03 at RMP #17 to 1.59 at RMP #23. The wall-pressure spectra shown in Fig. 14 can be related to the wake strength parameter: the larger Π is, the worse is the agreement between the reference wall-pressure spectra and Goody's model. It emphasizes the need of a wall pressure spectral model taking into account the effect of the mean pressure gradient.

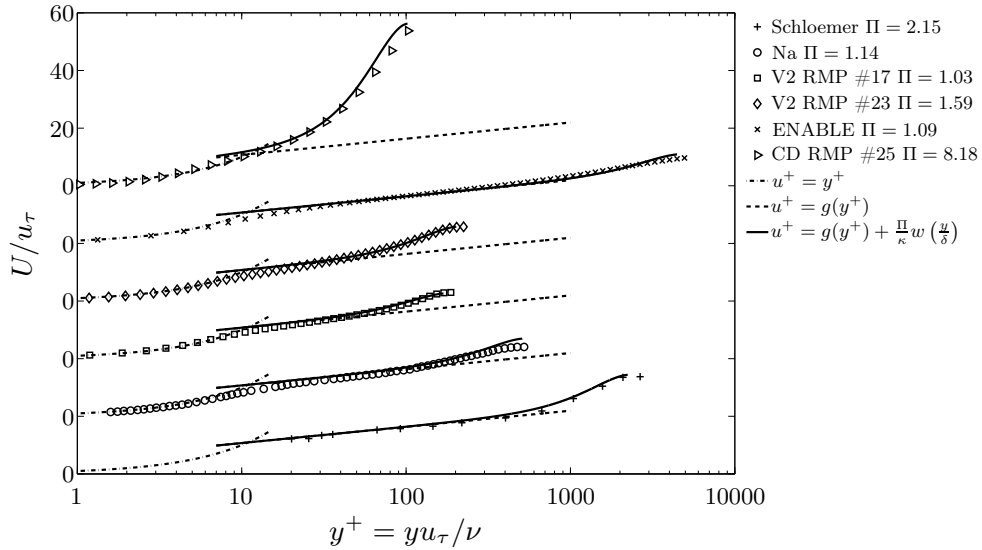


Fig. 13: Velocity profiles in wall units.

Velocity profiles experience a growing defect in the near-wall region as the adverse pressure gradient increases. The defect law defined as $(U_e - U)/U_e = f(y/\delta)$ shows large discrepancies for the 6 profiles in Fig. 15-(a). To obtain an outer velocity scale and to collapse velocity profiles in the outer region, Zagarola & Smits [46] have proposed a modified defect law. It has been initially developed for a pipe flow and favorably compared to experimental data. Zagarola-Smits' law is defined as $(U_e - U)/U_{ZS} = f(y/\delta)$, where $U_{ZS} = U_e \delta^*/\delta$. Maciel *et al.* [47] have also applied this defect law to different turbulent boundary layer with APG. Fig. 15-(b) shows Zagarola-Smits' defect law for the 6 velocity profiles. Na & Moin [7] do not provide the boundary layer thickness (δ) and so it has been deduced from the velocity profile, leading to an uncertainty of this quantity. It is not

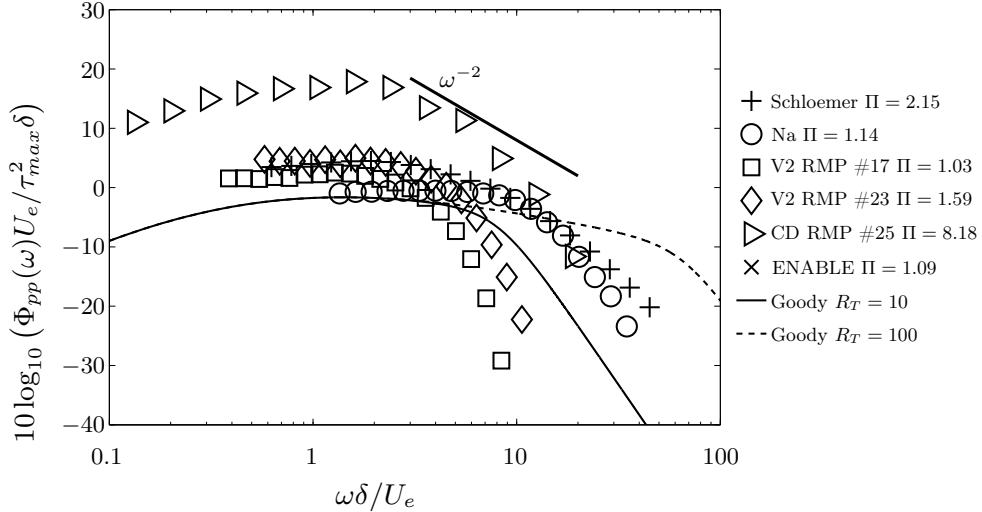


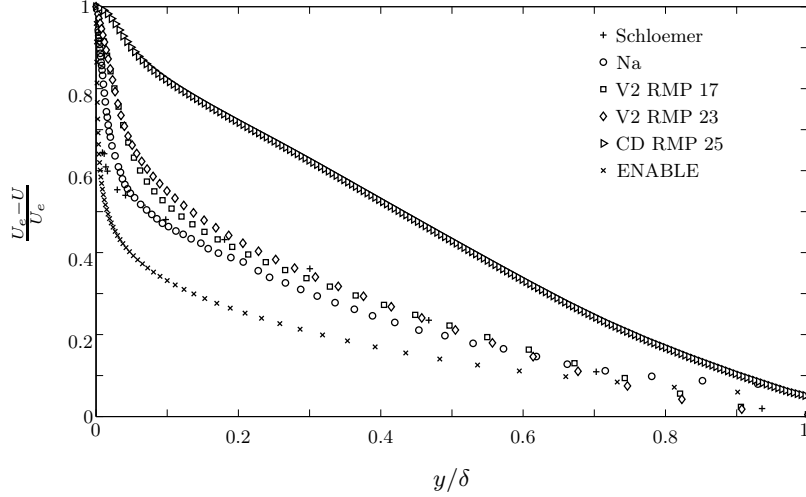
Fig. 14: Wall pressure spectra normalized by mixed variables using δ . APG spectra compared with Goody's model.

the case for the displacement and momentum thicknesses (δ^* and θ) in which we are more confident. Zagarola-Smits' defect law provides a better collapse than the classical defect law for the test-cases (results by Na excepted). Since it provides an auto-similarity of the velocity profile in the outer region (typically for $y/\delta > 0.2$), $\Delta = \delta/\delta^*$ is then considered as an other parameter characterizing the effect of the adverse pressure gradient.

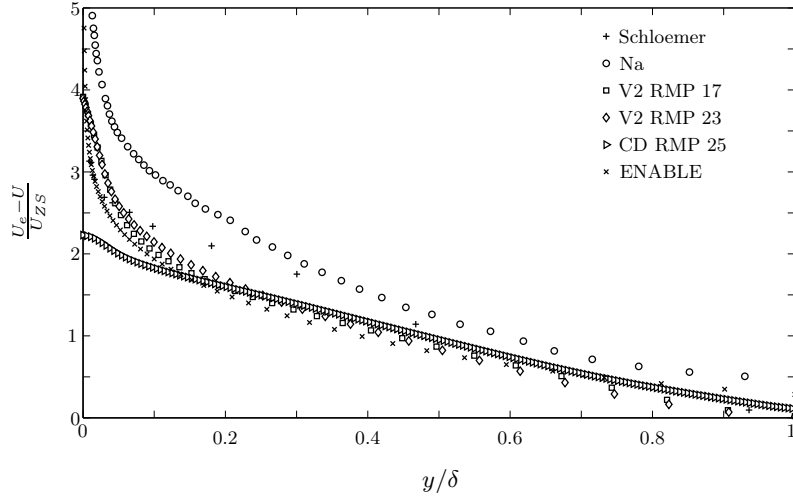
Clauser [48] defined the equilibrium parameter $\beta_C = (\theta/\tau_w)(dp/dx)$ to determine whether self-similarity has been achieved. Considering Clauser's definition, the test-cases boundary layers are not equilibrium ones. But the pressure gradient parameter β_C is of practical interest to quantify the local pressure gradient and will be used in the next section to develop the empirical spectral model. Whereas both Π and Δ are influenced by the boundary layer history, β_C is rather a local parameter.

IV. Empirical spectral model incorporating adverse mean-pressure gradient effects

The use of wall-pressure spectral models, as reviewed in section II, is not relevant to predict wall-pressure spectra of APG flows because it leads to a strong under-estimate, especially at low frequencies. Fig. 14 illustrates this phenomenon by comparing Goody's model with the APG spectra



(a) Classical defect law



(b) Zagarola-Smits' defect law

Fig. 15: Mean velocity in deficit coordinates.

from the test-cases. The discrepancies are important for boundary layers with strong APG, related to high values of Π and β_C . We propose a new model for APG wall-pressure spectra, based on Goody's model including the following corrections:

1. Displacement thickness δ^* is a more accurate data than the boundary layer thickness δ . The model will be normalized using the mixed variables and δ^* instead of δ .
2. As suggested by Simpson *et al.* [49], in APG flow, the maximum shearing stress along the normal $\tau_{max} = \max[\mu(dU/dy)]$ has to be preferred to the wall shear stress τ_w to scale the

pressure fluctuations.

3. Without any APG, the new model should collapse with Goody's model.
4. In the overlap region of APG flows, the spectral levels decay as $\omega^{-\alpha}$ with α which can be larger than 0.7 (see the -2 slope in Fig. 14).
5. As $\omega \rightarrow \infty$, spectral levels can decay faster than ω^{-5} , especially for the low Reynolds number flows. McGrath & Simpson [50] observed a slope -5.5 for $\omega\delta^*/U_e > 7$ (see also Figure 7 in [51]). When the high-frequency correction (due to the microphone spatial resolution) is significant, the slope at high frequency is difficult to evaluate. The larger correction is obtained for Schloemer's test-case where the attenuation is evaluated to be 9 dB for $\omega\delta^*/U_e = 8$, using the correction proposed by Corcos [16] with an equivalent radius [52] $r_{eq} = 0.62r$ and a convection velocity $U_c = 0.7U_e$.
6. The global level of fluctuating pressure increases as the pressure gradient parameters increase.

The first correction is applied by rewriting Goody's model with the boundary displacement thickness, assuming a 1/7th power law for a ZPG. In this particular case, $\Delta = \delta/\delta^* = 8$ and:

$$\frac{\Phi_{pp}(\omega)U_e}{\tau_{max}^2\delta^*} = \frac{C'_2(\omega\delta^*/U_e)^2}{\left[4.76(\omega\delta^*/U_e)^{0.75} + C'_1\right]^{3.7} + [C'_3(\omega\delta^*/U_e)]^7}, \quad (9)$$

with $C'_1 = 0.5$, $C'_2 = 1536$ and $C'_3 = 8.8R_T^{-0.57}$.

Based on the new formulation of Goody's model using the displacement thickness (Eq. 9), the derived functional form is:

$$\frac{\Phi_{pp}(\omega)U_e}{\tau_{max}^2\delta^*} = \frac{F_2(\Pi, \beta_C, \Delta)(\omega\delta^*/U_e)^2}{\left[4.76(\omega\delta^*/U_e)^{0.75} + F_1(\Pi, \beta_C, \Delta)\right]^{A_1} + [C'_3(\omega\delta^*/U_e)]^{A_2}}. \quad (10)$$

Firstly, the coefficients A_1 and A_2 that drive the slope respectively in the overlap and in the high frequency regions are deduced to meet the previous requirements, leading to

$$A_1 = 3.7 + 1.5\beta_C, \quad A_2 = \min\left(3, 19/\sqrt{R_T}\right) + 7$$

F_1 is then determined so that $\frac{\Phi_{pp}(\omega)U_e}{\tau_{max}^2\delta^*F_2(\Pi, \beta_C, \Delta)}$ is maximum for $\omega\delta/U_e = 1.4$ or equivalently for $\omega\delta^*/U_e = 1.4/\Delta$, as in Goody's model. A fairly accurate approximation is given by:

$$F_1 = 4.76 \left(\frac{1.4}{\Delta}\right)^{0.75} [0.375A_1 - 1] \quad (11)$$

$F_2 = F_{2a} \cdot F_{2b}$ is then determined by a two-step procedure. First, F_{2a} is calculated to satisfy $\left[10 \log_{10} \left(\frac{\Phi_{pp}(\omega) U_e}{\tau_{max}^2 \delta^*} \right)\right]_{max} \approx 7.4$ dB for $\omega \delta^*/U_e = 1.4$ assuming $F_{2b} = 1$. It assures for a zero pressure gradient spectrum to behave as Goody's model at low frequencies. Then $F_{2b} = 4.2 \left(\frac{\Pi}{\Delta} \right) + 1$ has been determined thanks to the 6 reference spectra presented in section III B. As the APG increases, Π increases and Δ decreases. Hence the idea to combine these effects and to define the variable Π/Δ .

The final proposed model is then fully determined by:

$$\frac{\Phi_{pp}(\omega) U_e}{\tau_{max}^2 \delta^*} = \frac{\left[2.82 \Delta^2 (6.13 \Delta^{-0.75} + F_1)^{A_1} \right] \left[4.2 \left(\frac{\Pi}{\Delta} \right) + 1 \right] \tilde{\omega}^2}{\left[4.76 \tilde{\omega}^{0.75} + F_1 \right]^{A_1} + \left[C_3' \tilde{\omega} \right]^{A_2}} \quad (12)$$

Figure 16 shows how the model behaves as the pressure gradient parameters vary. As Δ decreases, Π and β_C being held constants at non-zero values, the level of the normalized pressure spectrum is increased at mid and high frequencies whereas it decreases at low frequencies (cf. Fig. 16-(a)). In Fig. 16-(b), Δ is held constant as β_C increases. β_C and Π are correlated and can not vary independently. Durbin & Pettersson Reif [53] proposed the following empirical formula:

$$\Pi = 0.8(\beta_C + 0.5)^{3/4} \quad (13)$$

which is used to calculate Π in Fig. 16-(b). As Π and β_C increase, the maximum obtained at $\omega \delta^*/U_e = 1.4/\Delta$ is higher and the overlap region is decreased.

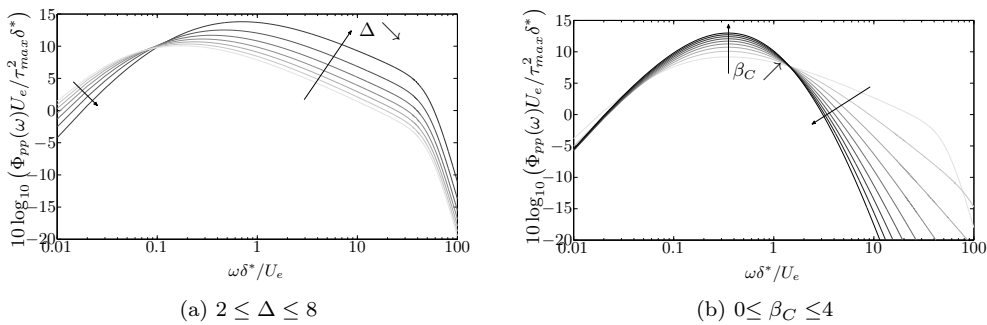


Fig. 16: Evolution of the wall-pressure spectral model with the adverse pressure gradient parameters.

V. Results

The model for APG wall pressure spectra is compared to the reference spectra in Fig. 17. The new model is in better agreement than Goody's model, which is an expected result since Goody's model is only valid for ZPG boundary layers. The agreement is poorer for flows with a mild pressure gradient (cf Fig. 17-(b) and 17-(c)).

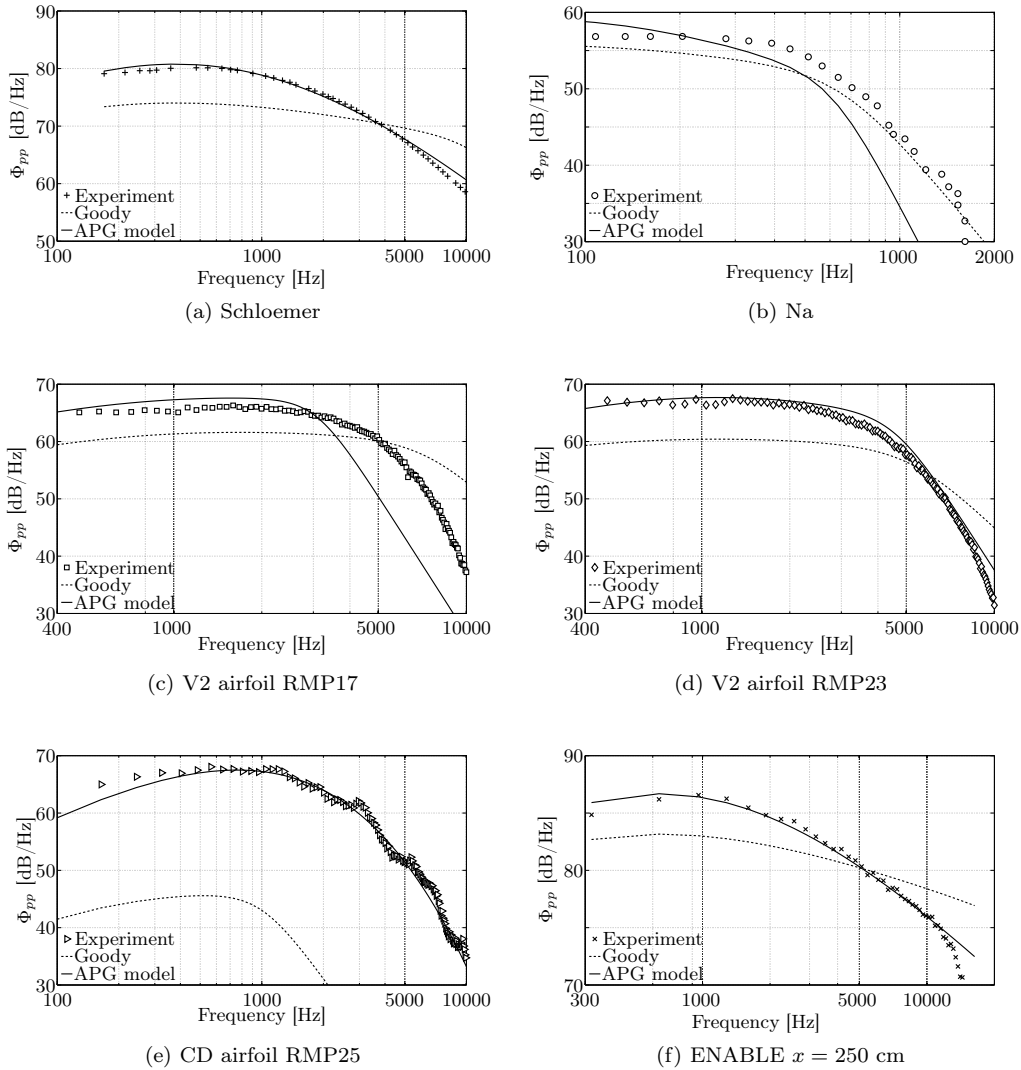


Fig. 17: Wall pressure spectra. Comparison between Goody's model and present model.

Knowing the wall pressure spectrum in the vicinity of the trailing edge and assuming an attached flow, the noise radiated as boundary layer vorticity is convected past the trailing edge of an airfoil can be predicted using analytical models [1, 3]. The coherence length scale l_y and the convection velocity

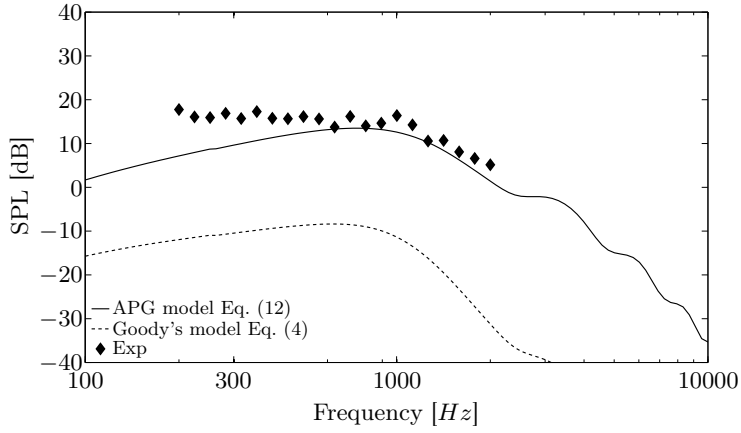


Fig. 18: Far field acoustic spectra in dB (integrated over 8 Hz bin width and reference to 2×10^{-5} Pa) in the midspan plane above the CD airfoil at a distance of 2 m. Experiment from Moreau & Roger[34] is compared to Amiet’s model.

U_c have also to be determined in order to predict the radiated noise using Amiet’s model [1]. The sound radiated in the mid-span plane by the CD airfoil has been measured by Moreau & Roger [34]. The microphone is placed at a distance $R = 2$ m above the airfoil trailing edge ($\theta = 90^\circ$). The results are presented in Fig. 18. At low and high frequencies, the signal-to-noise ratio is very low and the experimental data are limited to the range [200 Hz-2 kHz]. To predict the far-field noise analytically, the coherence length scale is determined by Corcos’ model:

$$l_y(\omega) = \frac{bU_c}{\omega} \quad (14)$$

with $U_c = 0.7U_i$ and $b = 1.47$, determined by post-processing experimental results [34]. For a loaded airfoil, the far-field pressure is strongly related to the wall pressure spectrum in the vicinity of the trailing edge on the suction side. Amiet’s model strongly underestimates the far field spectra if wall pressure spectra is determined using Goody’s model. With the new model for APG flows, the agreement is much better.

To demonstrate the ability of the model to predict the wall pressure spectrum of any flow encountering APG, it is evaluated on two demonstration cases not connected to the database. For the first case, the experimental data have been carried out in the anechoic wind tunnel at ECL. A NACA5510 profile with a 200 mm chord and a 200 mm span is placed into the core of a jet at

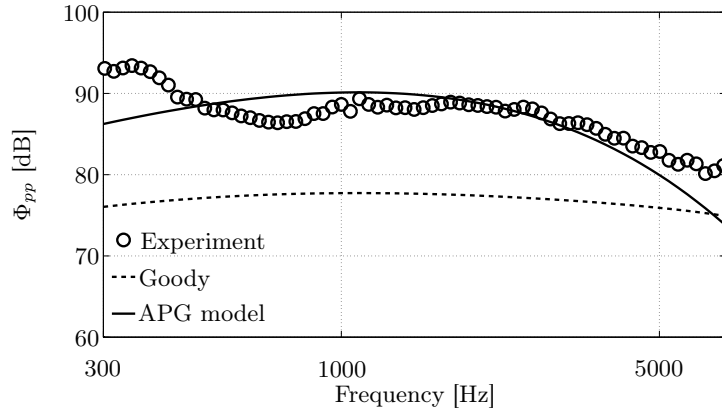


Fig. 19: Wall pressure spectrum in the aft region of a NACA5510 profile. Comparison between Goody's model and present model.

a reference velocity of 70 m/s. The angle of attack is 15° and we will focus on the results in the aft region of the suction side, where the pressure gradient is positive ($x/c = 95\%$). More details on the experimental setup are given by Jacob *et al.* [54]. This configuration has been numerically studied by Boudet *et al.* [55] following a classical RANS approach. The results of the numerical simulation are used as input data for the model and the comparison of the wall pressure spectrum at mid-span near the trailing edge is presented in Fig. 19. APG model is in better agreement with the experimental data than Goody's model.

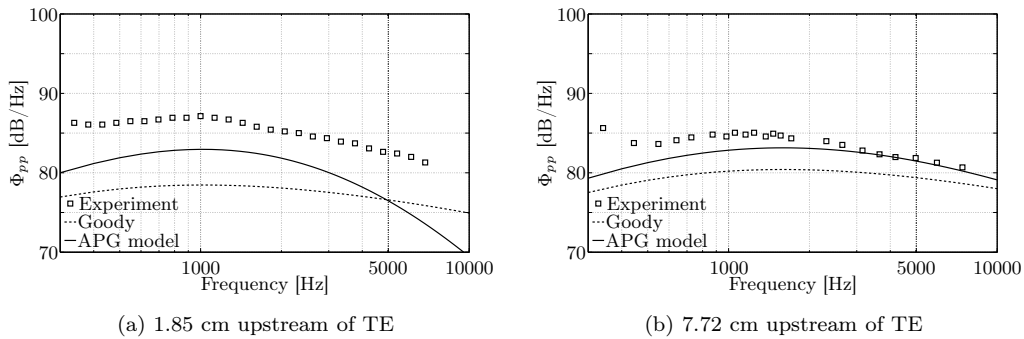


Fig. 20: NACA0012 wall pressure spectra. Goody's model, present model and experiments by Brooks & Hodgson [56].

Table 2: Inner and outer boundary-layer variables on Brooks & Hodgson’s NACA 0012. Results from XFOIL 6.9.

Distance upstream of TE	U_e (m/s)	δ (m)	δ^* (m)	θ (m)	H	τ_w (Pa)	β_C	Π	R_θ	Δ
$x_{TE} = 18$ mm	64.6	1.42×10^{-2}	2.36×10^{-3}	1.57×10^{-3}	1.49	5.43	3.51	1.56	6747	6.00
$x_{TE} = 77$ mm	69.3	0.97×10^{-2}	1.62×10^{-3}	1.12×10^{-3}	1.43	8.52	0.60	0.56	5145	6.00

The second demonstration case is the well-known NACA0012 experiment by Brooks & Hodgson [56]. The configuration with an angle of attack of 0° at 69.5 m/s with a sharp trailing edge is studied. This configuration enables the boundary layer parameters to be estimated by neglecting the installation effect. So XFOIL 6.9 is used to provide boundary layer displacement and momentum thicknesses, friction coefficient, external velocity and pressure distribution. The boundary layer thicknesses ratio ($\Delta = \delta/\delta^*$) is given by the experimental data of Garcia-Sagrado *et al.* [57] on the same airfoil at a lower Reynolds number. Boundary layer parameters are summarized in Table 2. Figure 20 compares the experimental wall pressure spectra to Goody’s and present models for two chordwise positions upstream of the trailing edge. For both locations, 1.8 cm and 7.7 cm upstream of the trailing edge ($x/c = 97\%$ and 87% respectively), Goody’s model underestimates pressure level of about 7 dB and 4 dB respectively. The APG model improves the prediction but is still lower than the experimental data. At 7.7 cm upstream of the trailing edge, the APG model is less than 2 dB below the experimental result and at 1.8 cm upstream of the trailing edge, it is between 3 dB and 5 dB below. The wall-pressure spectrum prediction is then improved by the APG model. Figure 21 shows that the use of the APG model improves the trailing-edge noise prediction based on Amiet’s theory.

VI. Conclusion

An extension of Goody’s model enabling the prediction of APG wall-pressure spectrum was developed and assessed on the basis of 6 test-cases. The model requires the knowledge of the mean steady flow field, more precisely the streamwise pressure distribution and the velocity profile normal

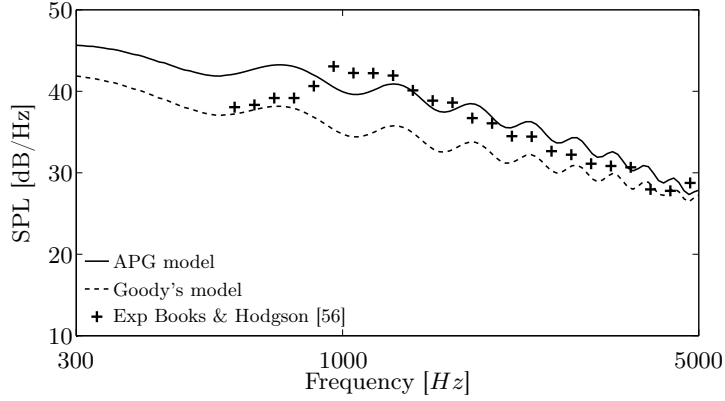


Fig. 21: Far field acoustic spectrum in the midspan plane at a distance $R = 1.2$ m above a NACA 0012 at $U_0 = 69.5$ m/s.

to the wall, given by a RANS simulation for instance. It is demonstrated that the effect of adverse pressure gradient can not be neglected, since it leads to an underestimate of the wall pressure spectrum directly affecting the far-field noise prediction when applied to the trailing-edge noise prediction. It is proposed that the more relevant parameters that drive the effects of the pressure gradient on the turbulent boundary layer are the wake strength parameter, Clauser's parameter and the ratio of the boundary-layer-to-displacement thicknesses. The APG model can be used for flows on the verge of separating, as long as they remain attached. It improves the pressure level prediction and the shape of the spectra, especially for high pressure gradient flows.

Only few studies have been published on APG flows in which both mean flowfield and wall-pressure fluctuations are provided. Further validation would benefit from new test-cases. Comparison to data for three-dimensional boundary layers are also warranted. It should also be noted that the model is limited to APG flows and cannot be applied to FPG flows.

The model can be used as post-processing of RANS simulations, which are affordable in industrial context for complex geometries. It is almost instantaneous and the total (RANS+postprocessing) computational costs are small compared with a LES. It can be coupled with analytical approaches to predict airfoil trailing-edge noise. The coupling with the extended Amiet's model to rotating blade, recently validated by Rozenberg *et al.* [58], would be an interesting study, especially for the prediction of wind turbine noise.

ACKNOWLEDGMENTS

The authors would like to thank Douglas Neal who carried out the hot-wire measurements on the controlled-diffusion airfoil at Michigan State University and Julien Christophe who provided the RANS simulation on the CD airfoil at von Karman Institute.

The data on the NACA5510 airfoil have been obtained in the framework of the EU project PROBAND. The authors would like to thank Marc Jacob and Julien Grilliat for the experimental results and Joëlle Caro for the RANS simulation.

REFERENCES

- [1] Amiet, R. K., “Noise due to turbulent flow past a trailing edge,” *J. Sound Vib.*, Vol. 47, No. 3, 1976, pp. 387–393.
- [2] Howe, M. S., “A review of the theory of trailing-edge noise,” *J. Sound Vib.*, Vol. 61, No. 3, 1978, pp. 437–465.
- [3] Howe, M. S., “Edge-source acoustic Green’s function for an airfoil of arbitrary chord, with application to trailing-edge noise,” *The quarterly Journal of Mechanics and Applied Mathematics*, Vol. 54, No. 1, 2001, pp. 139–155.
- [4] Roger, M. and Moreau, S., “Back-scattering correction and further extensions of Amiet’s trailing edge noise model. Part 1: Theory,” *J. Sound Vib.*, Vol. 286, No. 3, 2005, pp. 477–506.
- [5] Bull, M. K., “Wall-Pressure Fluctuations Beneath Turbulent Boundary Layers: Some Reflections on Forty Years of Research,” *J. Sound Vib.*, Vol. 190, No. 3, 1996, pp. 299–315.
- [6] Choi, H. and Moin, P., “On the Space-Time Characteristics of Wall-Pressure Fluctuations,” *Phys. Fluids A*, Vol. 2, No. 8, 1990, pp. 1450–1460.
- [7] Na, Y. and Moin, P., “The structure of wall-pressure fluctuations in turbulent boundary layers with adverse pressure gradient and separation,” *J. Fluid Mech.*, Vol. 377, 1998, pp. 347–373.
- [8] Sandberg, R. and Sandham, N., “Direct numerical simulations of turbulent flow past a trailing edge and the associated noise generation,” *J. Fluid Mech.*, Vol. 596, 2008, pp. 353–385.
- [9] Lee, Y. T., Blake, W. K., and Farabee, T. M., “Modeling of Wall Pressure Fluctuations Based on Time Mean Flow Field,” *ASME Journal of Fluids Engineering*, Vol. 127, No. 2, 2005, pp. 233–240.
- [10] Lee, Y. T., Farabee, T. M., and Blake, W. K., “Turbulence Effects of Wall-Pressure Fluctuations for Reattached Flow,” *Computers & Fluids*, Vol. 38, 2009, pp. 1033–1041.

- [11] Peltier, L. J. and Hambric, S. A., “Estimating Turbulent Boundary Layer Wall-Pressure Spectra from CFD RANS Solutions,” *Journal of Fluids and Structures*, Vol. 23, 2007, pp. 920–937.
- [12] Remmler, S., Christophe, J., Anthoine, J., and Moreau, S., “Computation of Wall-Pressure Spectra from Steady Flow Data for Noise Prediction,” *AIAA Journal*, Vol. 48, No. 9, 2010, pp. 1997–2007.
- [13] Panton, R. L. and Linebarger, J. H., “Wall Pressure Spectra Calculations for Equilibrium Boundary Layers,” *J. Fluid Mech.*, Vol. 65, No. 2, 1974, pp. 261–287.
- [14] Goody, M., “Empirical Spectral Model of Surface Pressure Fluctuations,” *AIAA Journal*, Vol. 42, No. 9, 2004, pp. 1788–1794.
- [15] Keith, W. L., Hurdis, D. A., and Abraham, B. M., “A Comparison of Turbulent Boundary Layer Wall-Pressure Spectra,” *ASME Journal of Fluids Engineering*, Vol. 114, No. 3, 1992, pp. 338–347.
- [16] Corcos, G. M., “Resolution of Pressure in Turbulence,” *J. Acoust. Soc. Am.*, Vol. 35, No. 2, 1963, pp. 192–199.
- [17] Hwang, Y. F., Bonness, W. K., and Hambric, A., “Comparison of semi-empirical models for turbulent boundary layer wall pressure spectra,” *J. Sound Vib.*, Vol. 319, 2009, pp. 199–217.
- [18] Willmarth, W. W. and Roos, F. W., “Resolution and Structure of the Wall Pressure Field Beneath a Turbulent Boundary Layer,” *J. Fluid Mech.*, Vol. 22, 1965, pp. 81–94.
- [19] Bakewell, H. P., Carey, G. F., Libuha, J. J., Schloemer, H. H., and Von Winkle, W. A., “Wall Pressure Correlations in Turbulent Pipe,” Tech. rep., USL Rpt. No. 559, 1962.
- [20] Bull, M. K., “Wall-Pressure Fluctuations Associated with Subsonic Turbulent Boundary Layer Flow,” *J. Fluid Mech.*, Vol. 28, No. 4, 1967, pp. 719–754.
- [21] Bull, M. K. and Thomas, S. W., “High Frequency Wall Pressure Fluctuations in Turbulent Boundary Layers,” *Phys. Fluids*, Vol. 19, No. 4, 1976, pp. 597–599.
- [22] Carey, G. F., Chlupsa, J. E., and Schloemer, H. H., “Acoustic Turbulent Water-Flow Tunnel,” *J. Acoust. Soc. Am.*, Vol. 41, No. 2, 1967, pp. 373–379.
- [23] Farabee, T. M., “An Experimental Investigation of Wall Pressure Fluctuations Beneath Non-equilibrium Turbulent Flows,” Tech. rep., DTNSRDC No. 86/047, 1986.
- [24] Keith, W. L. and Bennett, J. C., “Low Frequency Measurements of the Wall Shear Stress and Wall Pressure in a Turbulent Boundary Layer,” *AIAA Journal*, Vol. 29, No. 4, 1991, pp. 526–530.
- [25] Schewe, G., “On the structure and resolution of wall-pressure fluctuations associated with turbulent boundary-layer flow,” *J. Fluid Mech.*, Vol. 134, 1983, pp. 331–328.
- [26] Schloemer, H. H., “Effects of Pressure Gradients on Turbulent-Boundary-Layer Wall-Pressure Fluctuations,” *J. Acoust. Soc. Am.*, Vol. 42, No. 1, 1967, pp. 93–113.

- [27] Willmarth, W. W. and Wooldridge, C. E., “Measurements of the fluctuating pressure at the wall beneath a thick turbulent boundary layer,” *J. Fluid Mech.*, Vol. 14, 1962, pp. 187–210.
- [28] Chase, D. M., “Modeling the Wavevector-Frequency Spectrum of Turbulent Boundary Layer Wall Pressure,” *J. Sound Vib.*, Vol. 70, No. 1, 1980, pp. 29–67.
- [29] Howe, M. S., *Acoustics of Fluid-Structure Interactions*, Cambridge University Press, 1998.
- [30] Bradshaw, P., “‘Inactive’ motion and pressure fluctuations in turbulent boundary layers,” *J. Fluid Mech.*, Vol. 30, No. 2, 1958, pp. 241–258.
- [31] Na, Y., *Direct numerical simulation of turbulent boundary layers with adverse pressure gradient and separation*, PhD dissertation, Stanford University, 1996.
- [32] Robert, G., “Experimental database for the pressure gradient effect,” Tech. rep., UE Research Programme, Contract No. G4RD-CT-2000-00223, 2002.
- [33] Rozenberg, Y., Roger, M., and Moreau, S., “Effect of Blade Design at Equal Loading on Broadband Noise,” *Proceedings of the 12th AIAA/CEAS Aeroacoustics Conference, Cambridge, Massachusetts*, No. AIAA-2006-2563, 2006.
- [34] Moreau, S. and Roger, M., “Effect of Airfoil Aerodynamic Loading on Trailing-Edge Noise Sources,” *AIAA Journal*, Vol. 43, No. 1, 2005, pp. 41–52.
- [35] Spalart, P. R. and Watmuff, J. H., “Experimental and numerical study of a turbulent boundary layer with pressure gradients,” *J. Fluid Mech.*, Vol. 249, 1993, pp. 337–371.
- [36] Patel, V. C., “Calibration of the Preston tube and limitations on its use in pressure gradients,” *J. Fluid Mech.*, Vol. 23, 1965, pp. 185–208.
- [37] Klebanoff, P. S., “Characteristics of Turbulence in a Boundary Layer With Zero Pressure Gradient,” Tech. Rep. TR-1247, NACA, 1955.
- [38] Allen, J. M. and Tudor, D. H., “Charts for Interpolation of Local Skin Friction From Experimental Turbulent Velocity Profiles,” Tech. Rep. NASA SP-3048, NASA, 1969.
- [39] Moreau, S. and Roger, M., “Back-scattering correction and further extensions of Amiet’s trailing edge noise model. Part 2: Application,” *J. Sound Vib.*, Vol. 323, 2009, pp. 397–425.
- [40] Perennès, S. and Roger, M., “Aerodynamic Noise of a Two-Dimensional Wing with Highlift Devices,” *4th AIAA/CEAS Aeroacoustics Conference Meeting*, No. AIAA Paper 1998-2338, 1998.
- [41] Moreau, S., Henner, M., Iaccarino, G., Wang, M., and Roger, M., “Analysis of Flow Conditions in Freejet Experiments for Studying Airfoil Self-Noise,” *AIAA Journal*, Vol. 41, No. 10, 2003, pp. 1895–1905.
- [42] Menter, F. R., “Two-Equation Eddy-Viscosity Turbulence Models for Engineering Applications,” *AIAA Journal*, Vol. 32, No. 8, 1994, pp. 269–289.

- [43] Wang, M., Moreau, S., Iaccarino, G., and Roger, M., “LES prediction of wall-pressure fluctuations and noise of a low-speed airfoil,” *International Journal of Aeroacoustics*, Vol. 8, No. 3, 2009, pp. 177–197.
- [44] Christophe, J., Moreau, S., Hamman, C. W., Witteveen, J. A. S., and Iaccarino, G., “Uncertainty quantification for trailing-edge noise of a controlled-diffusion airfoil,” *Center for Turbulence Research, Proceedings of the Summer Program 2010*, 2010.
- [45] Coles, D., “The law of the wake in the turbulent boundary layer,” *J. Fluid Mech.*, Vol. 1, No. 2, 1956, pp. 191–226.
- [46] Zagarola, M. V. and Smits, A. J., “Mean-Flow scaling of turbulent pipe flow,” *J. Fluid Mech.*, Vol. 373, 1998, pp. 33–79.
- [47] Maciel, Y., Rossignol, K.-S., and Lemay, J., “Self-Similarity in the Outer Region of Adverse-Pressure-Gradient Turbulent Boundary Layers,” *AIAA Journal*, Vol. 44, No. 11, 2006, pp. 2450–2464.
- [48] Clauser, F. H., “Turbulent Boundary Layers in Adverse Pressure Gradients,” *Journal of the Aeronautical Sciences*, Vol. 21, No. 2, 1954, pp. 91–108.
- [49] Simpson, R. L., Ghodbane, M., and McGrath, B. E., “Surface pressure fluctuations in a separating turbulent boundary layer,” *J. Fluid Mech.*, Vol. 177, 1987, pp. 167–186.
- [50] McGrath, B. E. and Simpson, R. L., “Some Features of Surface Pressure Fluctuations in Turbulent Boundary Layers with Zero and Favorable Pressure Gradients,” Tech. rep., NASA CR-4051, 1987.
- [51] Goody, M. and Simpson, R. L., “Surface Pressure Fluctuations Beneath Two- and Three-Dimensional Turbulent Boundary Layers,” *AIAA Journal*, Vol. 38, No. 10, 2000, pp. 1822–1831.
- [52] Gilchrist, R. B. and Strawderman, W. A., “Experimental Hydrophone-Size Correction Factor for Boundary-Layer Pressure Fluctuations,” *The Journal of the Acoustical Society of America*, Vol. 38, 1965, pp. 298–302.
- [53] Durbin, P. A. and Reif, B. A. P., *Statistical Theory and Modeling for Turbulent Flows*, John Wiley & Sons, 2001.
- [54] Jacob, M. C., Grilliat, J., Camussi, R., and Caputi-Genaro, G., “Aeroacoustic investigation of a single airfoil tip leakage flow,” *International Journal of Aeroacoustics*, Vol. 9, No. 3, 2010, pp. 253–272.
- [55] Boudet, J., Grilliat, J., Caro, J., and Jacob, M. C., “Combined Experimental/Computational Study of Tip Clearance Flow and Acoustics,” *European Turbomachinery Conference*, 2009.
- [56] Brooks, T. F. and Hodgson, T. H., “Trailing Edge Noise Prediction from Measured Surface Pressures,” *J. Sound Vib.*, Vol. 78, No. 1, 1981, pp. 69–117.
- [57] Garcia Sagrado, A., Hynes, T., and Hodson, H., “Experimental Investigation Into Trailing Edge Noise Sources,” *Proceedings of the 12th AIAA/CEAS Aeroacoustics Conference, Cambridge, Massachusetts*,

No. AIAA-2006-2476, 2006.

- [58] Rozenberg, Y., Roger, M., and Moreau, S., “Rotating Blade Trailing-Edge Noise: Experimental Validation of Analytical Model,” *AIAA journal*, Vol. 48, No. 5, 2010, pp. 951–962.